RESEARCH ARTICLE

Stable, while Still Active? A DFT Study of Cu, Ag, and Au Single Atoms at the C_3N_4/TiO_2 Interface

Giovanni Di Liberto,[a] and Sergio Tosoni*[a]

[a] Dr. G. Di Liberto and Prof. S. Tosoni*
Department of Materials Science
University of Milan-Bicocca
Via Roberto Cozzi 55, 20125 Milan, Italy
E-mail: sergio.tosoni@unimib.it

Abstract: Hybrid DFT calculations are employed to compare the adsorption and stabilization of Cu, Ag, and Au atoms on graphitic C_3N_4 and on the heterojunction formed by g- C_3N_4 and TiO_2. While Cu and Ag can be strongly chemisorbed in form of cations on g- C_3N_4, Au is only weakly physisorbed. On g- C_3N_4/TiO_2, all coinage metal adatoms can be strongly chemisorbed, but, while Cu and Ag forms cations, Au form an Au^- species. Ab Initio Molecular Dynamics simulations confirm that the metal adatoms on g-C_3N_4 are highly mobile at room temperature, while they remain confined in the interfacial spacing between C_3N_4 and TiO_2 on the heterojunction, being both stably bound and reachable for the reactants in a catalytic cycle. Doping g-C_3N_4/TiO_2 with metal single atoms permits thus to generate catalytic systems with tunable charge and chemical properties and improved stability with respect to bare C_3N_4. Moreover, the changes in the electronic structure of g- C_3N_4/TiO_2 induced by the presence of the metal single atoms are beneficial also for photocatalytic applications.

Introduction

Single atom catalysts (SACs) are at the edge-cut of research in catalysis, thanks to their versatility and variety of potential applications, spanning from thermal catalysis, to organic synthesis, photocatalysis and electrocatalysis.[1–11] The key-concept behind the design of SACs is the idea to unify the advantages of homogeneous (and enzymatic) catalysis, where the active species is a single-metal atom bound to ligands, ensuring high activity, selectivity and chemical tunability, with the paradigmatic most favorable aspects of heterogeneous catalysis. In the latter case, the anchorage of the active catalytic species to a solid support permits to overcome the issues of dispersion and loss of the catalysts along the active cycle.[12] A wide range of different solid supports has been proposed to host single-atom active catalytic and electrocatalytic species, spanning from zeolites and metal-organic frameworks,[13–17] to oxides,[18–22] graphene[23–28] or other carbon-based materials, such as carbon nitride.[29–36]

SACs have attracted a lot of attention from computational groups over the last years due to their apparent simplicity: indeed, treating single metal atoms coordinated to model structures of simple surfaces is no big deal with nowadays computational facilities, in particular if the support is an atomic-thin two-dimensional material, such as graphene. However, an accurate analysis reveals how SACs are a highly non-banal system, where the actual chemical structure of the binding site, the computational description of the electronic structure of the metal-support complex, and the sampling of the potential energy surface are real challenges for simulation and thoroughly affect their predicting power.[37–39]

Recently, a strategy to improve the reactivity and stability of single-atom catalysts has begun to be explored, where the SAC is confined in the Van der Waals (VdW) spacing in layered materials, rather than bound to a surface.[40,41] For instance, Pt_1 single-atom species confined between SnS_2 layers were shown to outperform conventional carbon-based catalysts loaded with 10% Pt in the H_2 yield in the hydrogen evolution reaction (HER).[42] Similar, remarkable results for HER have been obtained for single platinum atoms dispersed in the VdW spacing in other layered materials[43] or, with a conceptually similar approach, in carbon nanotubes.[44] A stabilization of Pt_1 atoms, as well as a remarkable increase in the activity in the HER, was previously reported at the heterojunction between carbon nitride and zirconia.[45]

Beyond the case of the HER, single-atom species trapped in layered materials are currently investigated also in more involved organic synthetic processes,[46] as well as for applications in energy generation,[47] storage,[48] and as memristors.[49] In this paper, we explore, by means of state-of-the-art Density Functional Theory (DFT) simulations, a class of systems related to the 2D materials intercalated with single atoms: namely, we study the case where the single-atomic species are bound at the interface between two different materials, carbon nitride and titanium dioxide.

Heterojunctions formed by interfacing different materials, or even different facets of the same material,[50–57] are at the base of the strategy to improve the material's efficiency in sunlight exploitation and photocatalytic processes.[58–64] To this end, accurate computational studies are of great help in rationalizing the junction's effects in terms of band alignment,[65–68] surface terminations,[69] layer thickness[70,71] and role of point defects.[72]

In particular, the heterojunction formed by carbon nitride and titania displays very interesting features: upon exposition to visible light, charge carriers are generated and split in the two moieties following a direct Z-scheme. More precisely, experimental evidence indicates that the TiO_2 band edges are lower in energy than those of g-C_3N_4.[73] The photogenerated electrons in titania, with lower conduction band (CB), recombine

with the photogenerated holes in carbon nitride with a higher valence band (VB). In this way the photogenerated electrons in carbon nitride, with high reduction ability due to the higher CB, and the photogenerated holes in titania, with a high oxidation ability due to the lower VB, can be preserved. As proven in a previous computational work,[74] this mechanism is enabled by the formation of a strong interface dipole, related to the charge injection from carbon nitride to titania.

In the present work, we compare the bonding of copper, silver, and gold single atomic species on a free-standing g-C_3N_4 layer, and on the g-C_3N_4/TiO_2 heterojunction, seeing how chemical and electrostatic factors in the composite material affect the bonding strength and charge state of the transition metal (TM) adatoms. After discussing the simulated adsorption of TM adatoms by means of static calculations, their thermal stability at room temperature is analyzed recurring to Ab Initio Molecular Dynamics (AIMD) calculations. The computational details are provided at the end of the document.

Results and Discussion

Binding Cu, Ag and Au: Effect of the Substrate

The main results concerning the adsorption of the atom of free-standing and TiO_2-supported graphitic carbon nitride are reported in Table 1. A schematic picture of the encountered TM adsorption sites is provided in Figure 1. All structures have been fully relaxed with HSE06.

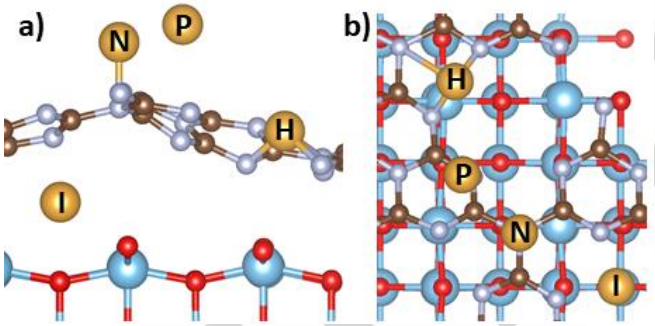

Figure 1. Visual description of all adsorption sites detected on g-C_3N_4/TiO_2: a) side view and b) top view. P: non-specific weak physisorption. N: top site on a nitrogen atom. H: heptazinic hollow site. I: in the interfacial spacing between C_3N_4 and TiO_2. Colour code: C (brown), N (cyan), O (red), Ti (light cyan), generic coinage metal adatom (gold).

Starting from copper, we observe that, on free-standing g-C_3N_4, the adatom forms a cation upon adsorption, transferring an electron to the conduction band of carbon nitride. This is assessed by inspecting the spin density and the atom-projected Density of States (p-DOS) in Figures 2a and 2b: indeed, the Cu adatom loses the spin density it has as an isolated gas species, owned to its $4s^1$, $3d^{10}$ electron configuration, while the trailing electron is delocalized in the conduction band of carbon nitride. The empty 4s orbital is also well evident in the PDOS plot. Two different adsorption sites are identified, in the heptazinic hollow (H) and on top of a nitrogen atom (N), Table 1 and Figures 2a, 2b. In both cases, a strong chemisorption takes place, with an adsorption energy of -2.32 eV (H) and -1.28 eV (N).

On the g-C_3N_4/TiO_2 heterostructure, the copper atom is further stabilized at the interface between titania and carbon nitride, and its binding energy increases to -3.96 eV and -3.17 eV when Cu is adsorbed at the interface between C_3N_4 and TiO_2 (site I, Figure 2c) or on the C_3N_4 hollow site (site H, Figure 2d). The Cu adatom is adsorbed as a mono-valent cation also on g-C_3N_4/TiO_2.

Table 1. Adsorption site, closest bond distance, estimated charge state, adsorption energy (D_e, eV) of Cu, Ag, and Au single atoms on free-standing g-C_3N_4, strained g-C_3N_4, and g-C_3N_4/TiO_2.

Atom	Support	Site[a]	Charge	D_e (eV)[b]
Cu	g-C_3N_4	H	+1	-2.32
		N	+1	-1.28
	g-C_3N_4/TiO_2	I	+1	-3.96
		H	+1	-3.77
Ag	g-C_3N_4	H	+1	-1.67
		P	0	-0.66
	g-C_3N_4/TiO_2	I	+1	-2.93
		P	0	-0.85
Au	g-C_3N_4	P1	0	-0.46
		P2	0	-0.49
	g-C_3N_4/TiO_2	P	0	-0.75
		H	-1	-1.67

[a] H: heptazinic hollow site. N: on top of a Nitrogen atom. P: physisorbed. I: g-C_3N_4/TiO_2 interface, see Fig. 1. [b] see the Computational Methods section for the actual definition of the adsorption energy.

Silver, compared to copper, has a higher ionization potential, which reflects in the charge states it can assume on the supports described here. On the free-standing g-C_3N_4, silver is adsorbed as a cation in the heptazinic pore with a strong De of -1.67 eV (H site, Figure 3a), or as a neutral atom with a moderate adsorption energy of -0.66 eV (site P, Figure 3b). When Ag is ionized, the spin density is visible on the g-C_3N_4 layer, Figure 3a, while the neutral state of the silver atom is evidenced by the spin density contour plot, which confirms that Ag maintains a ($5s^1$, $4d^{10}$) electron configuration, Figure 3b. In the case of the g-C_3N_4/TiO_2 interface, the positively charge Ag^+ (Figure 3c) undergoes a strong stabilization (D_e= -2.93 eV) as it is binds at the interface between g-C_3N_4 and TiO_2, (site I, Table 1) in direct contact to the oxygen atoms from the anatase surface. The physisorbed neutral Ag atom (site P, Figure 3d) is bound with a slightly larger D_e, -0.85 eV, compared to g-C_3N_4.

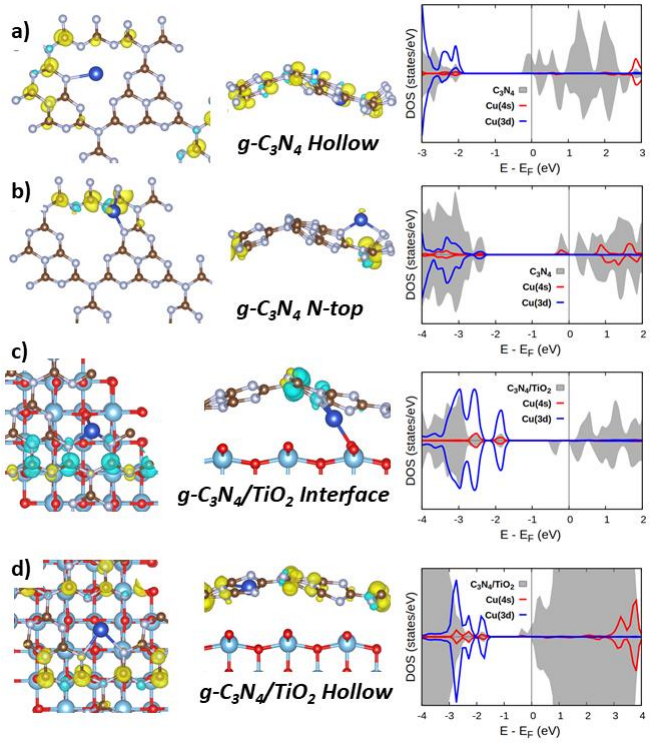

Figure 2. Cu adatom adsorbed on carbon nitride and carbon nitride/anatase heterostructure. Top view (left column), side view (middle column) and projected DOS (right column) of a) $Cu_1/g\text{-}C_3N_4$ (hollow site), b) $Cu_1/g\text{-}C_3N_4$ (nitrogen-top site), c) $Cu_1/C_3N_4/TiO_2$ (I site), d) $Cu_1/C_3N_4/TiO_2$ (H site). Colour code: C (brown), N (cyan), Cu (blue), O (red), Ti (light cyan). The spin density contour plot displays an isovalue of 0.005 |e| $Å^{-3}$: alpha and beta spin states are represented in yellow and cyan.

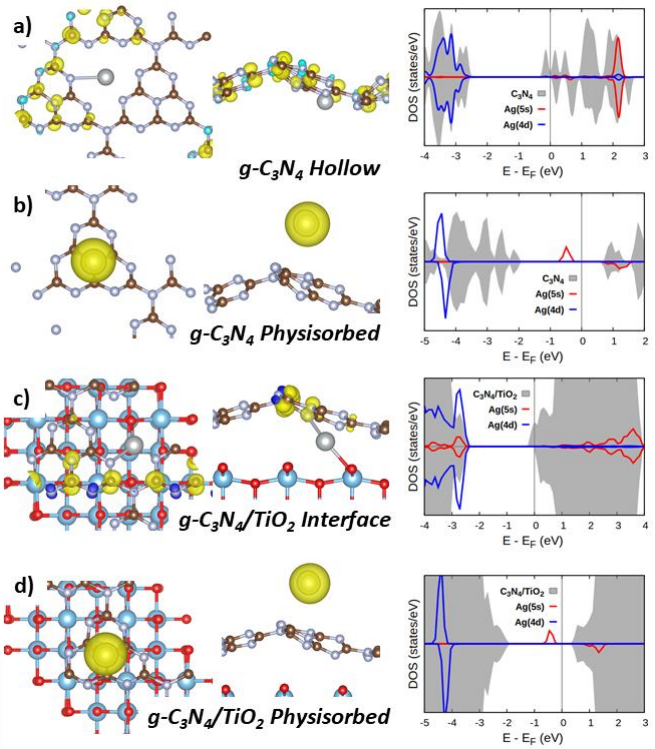

Figure 3. Ag adatom adsorbed on carbon nitride and carbon nitride/anatase heterostructure. Top view (left column), side view (middle column) and projected DOS (right column) of a) $Ag_1/g\text{-}C_3N_4$ (hollow site), b) $Ag_1/g\text{-}C_3N_4$ (physisorbed), c) $Ag_1/C_3N_4/TiO_2$ (I site), d) $Ag_1/C_3N_4/TiO_2$ (physisorbed). Colour code: C (brown), N (cyan), Ag (silver), O (red), Ti (light cyan). The spin density contour plot displays an isovalue of 0.005 |e| $Å^{-3}$: alpha and beta spin states are represented in yellow and cyan.

Gold has a stronger noble character with respect to silver and copper, which also translates into a less pronounced tendency to bind to the surface. Moreover, it displays also a higher electron affinity and a higher ionization potential compared to the other elements from group 11. This can be seen in the case of free-standing $g\text{-}C_3N_4$, where no cases of chemisorption of Au are observed, and only two slightly different structures where the adatom is physisorbed are identified, with similar D_e (-0.46 eV and -0.49 eV), Figures 4a and 4b. In both cases, the gold adatom is adsorbed as a neutral species. When gold binds to the $g\text{-}C_3N_4/TiO_2$ heterojunction, a local minimum where gold is physisorbed with D_e= -0.75 eV (slightly larger than on carbon nitride) can be found, Figure 4c. However, if gold is strongly chemisorbed on the heterostructure, Figure 4d, two relevant differences with respect to Cu and Ag can be appreciated, namely (i) gold is stabilized in the heptazinic pore of carbon nitride, rather than spontaneously penetrating into the interfacial spacing and (ii) gold tends to withdraw an electron from $g\text{-}C_3N_4/TiO_2$, form an Au^- anion. In analogy with the previous cases of Cu and Ag, however, a strong increase in the adsorption energy is observed, indicating a remarkable stabilization of the adatom on the heterostructure, compared to bare carbon nitride.

The data reported so far can be rationalized and discussed under the light of the different chemical nature of the adatoms and the adopted supports. Graphitic carbon nitride is a monolayer characterized by a buckled structure, displaying a porous motif. Its electronic structure shows a semiconducting character, where the valence and conduction bands are delocalized over the C and N atoms with bonding and antibonding character, respectively, reflecting the covalent nature of this material. The pores are ideal sites to stabilize adatoms and molecules, as widely studied in high-throughput computational works.[75] In the present work we notice as well that the coordination of metal adatoms on hollow site on $g\text{-}C_3N_4$ seems to more favorable than other possible adsorption modes (such as bond on N-top sites or non-specific physisorption). However, carbon nitride remains a graphitic-like, layered material, and the possibility that adatoms are stabilized as interstitial species between the C_3N_4 layers cannot be neglected.[76] This aspect, however, goes beyond the scope of the present work, where we would rather focus on the stabilization of the adatoms at the $g\text{-}C_3N_4/TiO_2$ interface. As explained in details elsewhere,[74] anatase TiO_2 and carbon nitride form a type-II (staggered gap) heterojunction, where the VB and CB edges of C_3N_4 lie above those of TiO_2. When the contact between the two

moieties is established, some negative charge flows from carbon nitride to titania, causing a net polarization of the interface. When TM adatoms are adsorbed on g-C_3N_4/TiO_2, thus, they interact with a substrate which, (i) presents different binding sites with respect to free-standing g-C_3N_4, for instance involving also oxygen atoms at the titania surface, ii) displays a down-ward oriented interfacial dipole moment, related to the charge depletion on the g-C_3N_4 side and accumulation at the TiO_2 side, and iii) has an electronic structure which remarkably differs from those of its separated units: the overall band gap of the g-C_3N_4/TiO_2 interface, notably, is around 2 eV, remarkably smaller than those of carbon nitride and titania, a fact with relevant implications to the establishment of new bonds with a strong charge transfer character upon adsorption of TM adatoms. Indeed, all these factors play a role in determining the binding of Cu, Ag, and Au single atoms.

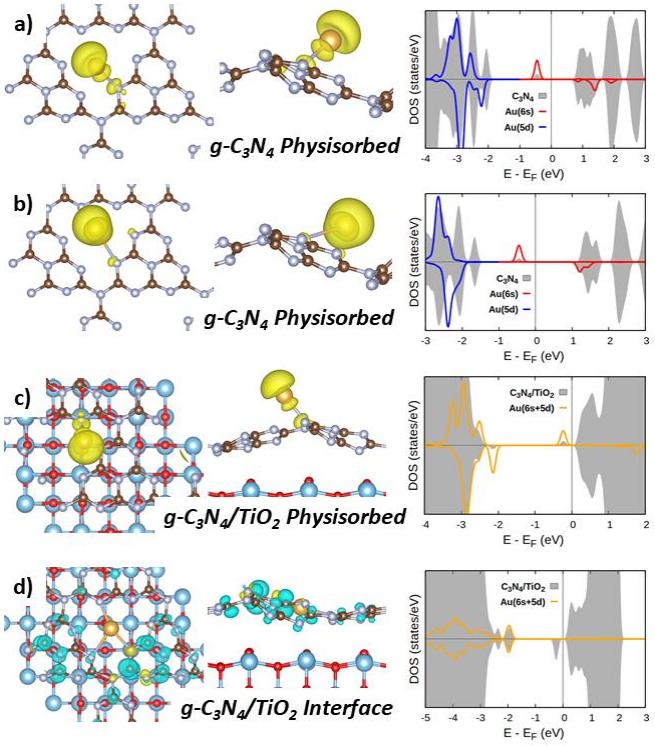

Figure 4. Au adatom adsorbed on carbon nitride and carbon nitride/anatase heterostructure. Top view (left column), side view (middle column) and projected DOS (right column) of a) Au_1/g-C_3N_4 (P1 configuration), b) Au_1/g-C_3N_4 (P2 configuration), c) Au_1/C_3N_4/TiO_2 (phisysorbed), d) Au_1/C_3N_4/TiO_2 (I site). Colour code: C (brown), N (cyan), Au (gold), O (red), Ti (light cyan). The spin density contour plot displays an isovalue of 0.005 |e| $Å^{-3}$: alpha and beta spin states are represented in yellow and cyan.

An interesting question is how the presence of TM adatoms influences the photocatalytic properties of C_3N_4/TiO_2. Some relevant hints in this respect can be derived analyzing the results presented here, even though they are all ground-state calculations, and no explicit treatment of the electronic excitations is considered. A first aspect is the change in the electronic structure induced by the bonding of the TM adatom. In the case of Cu, the positive ionization of the metal species generates deep occupied states localized on the metal center and shallow occupied states close to the conduction band edge, which, based on the spin density plots, are delocalized over the whole carbon nitride structure (Figures 2c and 2d). This could enhance the photogeneration of charge carriers by absorbing photons in the visible frequency range. Moreover, the dipole moment of the heterojunction (oriented with the negative pole on TiO_2 and the positive pole on C_3N_4), previously calculated as -0.25 |e| × Å,[74] is even more negative for Cu_1/g-C_3N_4/TiO_2 (-0.45 |e| × Å for I site, Figure 2c, and -0.41 |e| × Å for H site, Figure 2d). The increased negative dipole at the interface determines the mechanism for the recombination of the photoexcited charge carriers, furtherly corroborating the Z-scheme model previously prosed for the g-C_3N_4/TiO_2 heterojunction. The presence of Cu adatoms, thus, does not only improve the absorption properties of the heterojunction, but also facilitate the separation of high-energy charge carriers. For chemisorbed Ag, Figure 3c, the occupied 4d states from Ag fall within the TiO_2 valence band, and thus they do not alter the electronic structure in the gap region. Upon ionization to Ag^+, however, shallow occupied states delocalized over C_3N_4 appear close the conduction band edge. The interfacial dipole moment is -0.35 |e| × Å, larger compared to the adatom-free heterojunction, but smaller compared to the case of Cu. One can thus predict that doping the g-C_3N_4/TiO_2 interface with silver will have similar, though smaller, effects on the photocatalytic properties than doping with Cu. Notably, the “P” case where Ag is barely physisorbed without any charge transfer, Figure 3d, is not worth being discussed here: the band edges of the heterojunctions are almost unaffected by the presence of the metal, so is the interfacial dipole, and any photocatalytic mechanism involving exclusively the Ag states would have an intrinsically low quantum yield, due to the relatively small silver loading on the heterostructure. In the case of Au, the chemisorption of the adatom on g-C_3N_4/TiO_2 leads to the formation of an Au^- anion, Figure 4d. Here, the projected DOS shows the doubly occupied Au 6s state just above the valence band, while the hole created in the C_3N_4 moiety upon charge transfer to Au^- leaves a singly occupied state in the middle of the gap. It is worth reporting the strong decrease in the negative interfacial dipole, -0.16 |e| × Å, which may suggest that a type-II recombination scheme of the charge carrier may be preferred to the direct Z-scheme in this case.

A further worth-mentioning aspect is that, in case of adsorption of TM atoms in neutral state, or as negatively charged Au^- species, the Fermi level of the TM/C_3N_4/TiO_2 structures lie in the range between -4.8 eV and -4.5 eV with respect to the vacuum level, i.e. at energies which are only a small fraction of eV below the H^+/H_2 reduction potential, commonly referred to as the Standard Hydrogen Electrode (SHE), which DFT calculations typically locate in the range 4.8-4.3 eV below the vacuum level.[77] However, when the TM atom (Cu, or Ag) is positively charged, and an electron is transferred to the substrate, the Fermi level of the n-doped C_3N_4/TiO_2 heterojunction is significantly shifted in energy up -3.8 eV with respect to vacuum (Cu and Ag in interfacial sites), or even -3.3 eV (Cu at the hollow site). This fact indicates that this type of structures displays a strong reductive potential,

which may be suitable in photocatalytic applications oriented to the HER, for instance.

Dynamic Behaviour of SACs at Room Temperature

From the conceptual viewpoint, there are little doubts that SACs are potentially powerful catalytic systems, joining the advantages of homogeneous catalysis (undercoordinated metal atoms with tunable ligand effects to optimize their activity and selectivity) and heterogeneous catalysts (anchorage of the active species on a solid substrate, ensuring durability and reusability of the catalysts through several cycles). The SAC's nature of single, reactive atomic species, displaying high surface energy,[78] however, is also the main factor potentially hindering their application: indeed, single atoms are prone to aggregate or be cleaved out in the reaction's environment, if they are displaced from their bonding site. To assess the stability of the single-atom species described here, we now discuss the results from AIMD calculations performed at room temperature over a trajectory of 3 ps. One must consider that longer trajectories should be needed for a full sampling of the behavior of a catalytic system. However, few-ps long trajectories allow to gain some information on the surface chemistry of catalytic objects.[79–82] In the present case, we aim at extracting some information on the fluxionality of the supported metal atoms, and few ps-length trajectories can be considered adequate in this respect. To this end, we focus on the most stable case for each SAC, on each support (g-C_3N_4, and at the g-C_3N_4/TiO_2 heterojunction). In Table 2, the data concerning the bond distances for the TM adatom over the MD run are reported. In Figure 5, the closest bonding distance between the TM adatom and an atom on the support is reported all over the MD trajectory. For Cu on graphitic carbon nitride, the closest bonding distance between the SAC and the support oscillates between 1.84 Å and 2.19 Å over the MD run, with a mean value of 2.07 Å. This indicates a rather dynamic behavior of the Cu adatom, which moves in and out from the heptazinic pore, oscillating between two N atoms, as shown in the plot reported in Figure 5a, and passing from a strong bond situation to a much loose coordination. One can thus infer that this may indicate a loss of the TM adatom. The situation is quite different when the Cu adatom is stabilized on the g-C_3N_4/TiO_2 heterojunction: here, <R> is definitely short, 1.85 Å, indicating a strong bonding situation. The minimum and maximum bonding distances observed over the MD run are 1.71 Å and 1.97 Å respectively, much shorter than the previous case. Interestingly, as shown in Figure 5b. both short Cu-N and Cu-O bonds are preserved during the MD run, confirming how both components of the heterojunction contribute in stabilizing the Cu adatom, which, however, preserves a certain mobility within the Van der Waals spacing separating carbon nitride from titania.

A similar picture is reported for Ag. Here, the adatom is very weakly bound to the nitrogen atoms surrounding the heptazinic cavity on g-C_3N_4, as stated by the mean (2.38 Å), minimum (2.24 Å) and maximum (2.52 Å) Ag-N bonding distances observed along the MD trajectory. The mobile character of the Ag adatom is evident also from the plot in Figure 5c, showing how the TM species is oscillating between three N sites along the heptazinic cavity. Just like in the case of Cu, however, a much tighter bonding is reported on the heterojunction between carbon nitride and titania, Table 2 and Figure 5d, with Ag-N and Ag-O bonding distances oscillating between 1.73 Å and 1.97 Å (<R>= 1.86 Å). The scan over the MD trajectory in Figure 5d shows how the silver adatom remains in the proximity of the same O site, while two nearby N atoms on carbon nitride contribute to its stabilization.

Gold, with respect to copper and silver, has a more pronounced noble character and is thus less prone to be strongly anchored on carbon-based or oxidic supports. This definitely holds true also on g-C_3N_4, where Au is loosely bound across the heptazinic pores, with rather large average (2.25 Å), minimum (2.14 Å), and maximum (2.36 Å) bond distances. The plot in Figure 5e reveals the large variability undergone by the Au-N bonding distance, which emphasizes the mobility of the gold species at 300 K. The MD trajectory on the g-C_3N_4/TiO_2 heterojunction starts from a configuration where Au is bound to a nitrogen atom in the heptazinic pore. However, during the run, Au diffuses in the Van der Waals spacing between titania and carbon nitride, and also Au-O bonds are established, as clearly revealed in the plot in Figure 5f, with an average bond distance of 2.08 Å along the trajectory, and a minimum distance of 1.87 Å, much shorter compared to what reported for the free-standing carbon nitride. In Figure 5f, the shortest Au-N and Au-O distances are plotted for simplicity, because the SAC tends to jump between various nearby N-atoms. Notably, the adsorption energy of Au at the interface is almost identical to the pore site.

Table 2. Mean (<R>, Å), minimum (R^{min}, Å), and maximum (R^{max}, Å) bond distances across the MD trajectories for Cu, Ag and Au atoms bound on g-C_3N_4 and g-C_3N_4 /TiO_2.

Atom	Support	<R> (Å)	R^{min} (Å)	R^{max} (Å)
Cu	g-C_3N_4	2.07	1.84	2.19
	g-C_3N_4/TiO_2	1.85	1.71	1.97
Ag	g-C_3N_4	2.38	2.24	2.52
	g-C_3N_4/TiO_2	1.86	1.73	1.97
Au	g-C_3N_4	2.25	2.14	2.36
	g-C_3N_4/TiO_2	2.08	1.87	2.40

It appears thus evident that the titania-carbon nitride composite displays an intriguing trapping and stabilizing capability toward TM adatoms, which is here shown not only for a rather reactive species such as Cu, but also for a rather noble one, such as Au. Adatoms are confined in the Van der Waals spacing, and tend to oscillate between the carbonaceous and the oxidic moieties of the heterojunction, finding stable trapping sites on both sides. In the same time, the porous morphology of carbon nitride ensures that the catalytic active species are reachable for the reactant molecules. Further, intriguing developments of this work may investigate how the steric constrain exerted by the carbon nitride layer influences the selectivity and the reaction paths on the SACs stabilized at the interface.

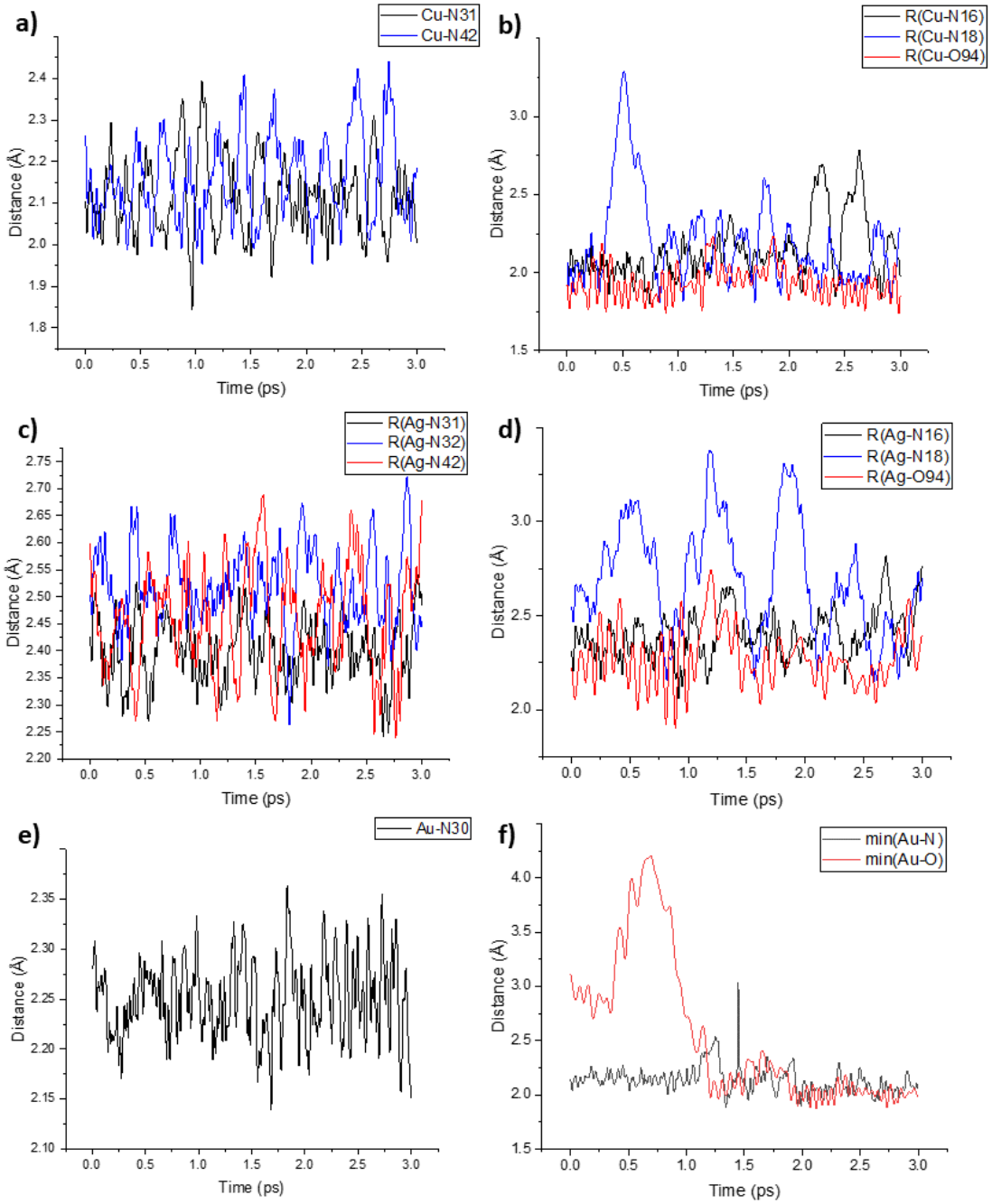

Figure 5. Minimum TM-X distance (TM=Cu, Ag, Au and X= N or O atom from the support) along the MD trajectories for a) $Cu_1/g\text{-}C_3N_4$ (hollow site), b) $Cu_1/C_3N_4/TiO_2$ (I site), c) $Ag_1/g\text{-}C_3N_4$ (hollow site), d) $Ag_1/C_3N_4/TiO_2$ (I site), e) $Au_1/g\text{-}C_3N_4$ (hollow site), f) $Au_1/C_3N_4/TiO_2$ (I site).

Conclusions

In this paper, the adsorption of Cu, Ag, and Au single atomic species has been studied on g-C_3N_4 and on the g- C_3N_4/TiO_2 heterojunction. On g- C_3N_4, Cu and Ag can be stabilized in form of monovalent cations, while Au is only weakly physisorbed as a neutral species. The picture radically changes on g- C_3N_4/TiO_2, where stable Cu^+, Ag^+, and Au^- can be formed, by exchanging electrons with the substrate. Both N atoms from the carbon nitride moiety and oxygen atoms from titania contribute in stabilizing the single metal species.

The ions chemisorbed on g- C_3N_4 display a remarkably large binding energy at 0 K, but, as evidenced with an MD simulation at room temperature, they can easily escape from their bonding site, suggesting a highly dynamic behavior, prone to a remarkable loss of catalytic material under operating conditions. In this respect, the C_3N_4/TiO_2 heterojunction is a definitely better support, since, at RT, the ions tend to remain confined in the Van der Waals spacing between carbon nitride and titania, and the contact to the support is well maintained. The porous nature of g-C_3N_4, moreover, ensures that the active single-metal species will be reachable, even when they are trapped between carbon nitride and titania.

A relevant aspect highlighted in this paper is the beneficial role of Cu species to the photocatalytic properties of g-C_3N_4/TiO_2. On the one hand, the charge injected from the Cu atoms to the support populate shallow state close to the conduction band, effectively reducing the band gap. On the other, the presence of the Cu^+ atoms actually increase the negative interfacial dipole moment, strengthening the direct Z-scheme which ensures separation of highly reactive charge carriers. A similar behavior, but up to a smaller extent, is expected for Ag^+. Au^-, on the contrary, induces deeper gap states, and determines a drastic reduction of the interfacial dipole moment, which should lead to a type-II behavior, rather than a direct Z-scheme.

Computational Methods

Spin-polarized Density Functional Theory calculations are performed recurring to the code VASP 6.[83–85] The interaction between the nuclei and the core electrons is modelled recurring to the Projector Augmented Wave approach.[86,87] C (2s,2p), N (2s, 2p), O (2s, 2p), Ti (4s, 3d), Cu (4s, 3d), Ag (5s, 4d), and Au (6s, 5d) electrons are treated explicitly in the electronic structure calculations. At first, static relaxations and subsequent analysis of the Density of States (DOS), spin density, and charge of the TM single atoms are performed recurring to the hybrid HSE06 functional.[88] Long-range dispersion forces are considered recurring to the damped DFT-D3 approach.[89,90] A mesh of 1x2x1 special K-points is used for free-standing g-C_3N_4, while the sampling was reduced to the Γ point for g- C_3N_4/TiO_2. A kinetic energy cutoff of 400 eV is used to expand the plane-wave basis set. Truncation criteria of 10^{-5} eV (electronic loop) and 10^{-2} eV/Å (ionic loop) are adopted. Dipole and quadrupole corrections are applied along the non-periodic direction. An empty space of at least 15 Å is included in the supercell to avoid spurious interactions between replicas of the slab. On the most stable structures obtained from the static calculations, Ab Initio Molecular Dynamics (AIMD) at a constant temperature of 300 K is performed using a canonical ensemble over a 3 ps trajectory after equilibration, with a time-step of 1 fs adopting the Generalized Gradient Approximation (GGA) functional PBE,[91] because of the high computational effort requested by AIMD simulations with hybrids. The Temperature was controlled by a Nosé-Hoover thermostat.[92,93]

For free-standing g-C_3N_4, a 1×2 supercell is adopted to simulate the adsorption of the TM adatoms on the graphitic monolayer. Based on previous findings, the corrugated heptazine structure is adopted.[74,94,95] The g-C_3N_4/TiO_2 heterostructure is modelled by superimposing a corrugated, heptazinic carbon nitride monolayer on an anatase TiO_2 (001) slab. The choice of the anatase surface is motivated by previous experimental data.[96] The lattice mismatch is minimized by adapting the g- C_3N_4 lattice parameters to those of anatase and searching for the best possible reciprocal rotation, with a residual strain of 7% and 2% along the two in-plane crystallographic directions. All details on the construction of the interface are reported in a previous publication from the group.[74]

The adsorption energy, D_e, is defined as follows:

$$D_e = E(adatom@substrate) - (E(substrate) + E(adatom))$$

where the adatom is adsorbed transition-metal species (Cu, Ag, or Au), while the substrate is either the free-standing or the titania-supported carbon nitride. The energy of the TM adatoms is estimated from their respective bulk cohesive energies. Negative values of D_e implies stable binding of the adatoms.

Acknowledgements

ST acknowledges financial support from Fondazione Cariplo, grant 2022-0713 PLANET ("Photocatalytic recovery of iodine from iodinated waste using single-atom catalysts"). GDL acknowledges the support from UNDERSAC and SACtoH2 projects funded by MUR. We acknowledge the CINECA award under the ISCRA initiative, for the availability of high-performance computing resources and support.

Keywords: DFT • Single-Atom Catalysts • Heterojunctions • Catalysis • Photocatalysis

References

[1] B. Qiao, A. Wang, X. Yang, L. F. Allard, Z. Jiang, Y. Cui, J. Liu, J. Li, T. Zhang, *Nat Chem* **2011**, *3*, 634–641.
[2] L. Liu, A. Corma, *Nat Rev Mater* **2021**, *6*, 244–263.
[3] C. Copéret, A. Comas-Vives, M. P. Conley, D. P. Estes, A. Fedorov, V. Mougel, H. Nagae, F. Núñez-Zarur, P. A. Zhizhko, *Chem Rev* **2016**, *116*, 323–421.
[4] G. Di Liberto, I. Barlocco, L. Giordano, S. Tosoni, G. Pacchioni, *Curr Opin Electrochem* **2023**, *40*, 101343.
[5] M. A. Bajada, J. Sanjosé-Orduna, G. Di Liberto, S. Tosoni, G. Pacchioni, T. Noël, G. Vilé, *Chem Soc Rev* **2022**, *51*, 3898–3925.
[6] M. A. Bajada, G. Di Liberto, S. Tosoni, V. Ruta, L. Mino, N. Allasia, A. Sivo, G. Pacchioni, G. Vilé, *Nature Synthesis* **2023**, *2*, 1092–1103.
[7] G. Vilé, G. Di Liberto, S. Tosoni, A. Sivo, V. Ruta, M. Nachtegaal, A. H. Clark, S. Agnoli, Y. Zou, A. Savateev, M. Antonietti, G. Pacchioni, *ACS Catal* **2022**, *12*, 2947–2958.
[8] A. Wang, J. Li, T. Zhang, *Nat Rev Chem* **2018**, *2*, 65–81.
[9] S. K. Kaiser, Z. Chen, D. Faust Akl, S. Mitchell, J. Pérez-Ramírez, *Chem Rev* **2020**, *120*, 11703–11809.
[10] H. Xu, Y. Zhao, Q. Wang, G. He, H. Chen, *Coord Chem Rev* **2022**, *451*, 214261.
[11] B. Singh, M. B. Gawande, A. D. Kute, R. S. Varma, P. Fornasiero, P. McNeice, R. V. Jagadeesh, M. Beller, R. Zbořil, *Chem Rev* **2021**, *121*, 13620–13697.
[12] C. Copéret, M. Chabanas, R. Petroff Saint-Arroman, J. Basset, *Angewandte Chemie International Edition* **2003**, *42*, 156–181.
[13] T. Zhang, Z. Chen, A. G. Walsh, Y. Li, P. Zhang, *Advanced Materials* **2020**, *32*, DOI 10.1002/adma.202002910.
[14] V. Hasija, S. Patial, P. Raizada, A. Aslam Parwaz Khan, A. M. Asiri, Q. Van Le, V.-H. Nguyen, P. Singh, *Coord Chem Rev* **2022**, *452*, 214298.
[15] M. Lu, M. Zhang, C. Liu, J. Liu, L. Shang, M. Wang, J. Chang, S. Li, Y. Lan, *Angewandte Chemie* **2021**, *133*, 4914–4921.
[16] J. Wang, Z. Zhang, Y. Li, Y. Qu, Y. Li, W. Li, M. Zhao, *ACS Appl Mater Interfaces* **2022**, *14*, 1024–1033.
[17] I. Barlocco, G. Di Liberto, G. Pacchioni, *Energy Advances* **2023**, DOI 10.1039/D3YA00162H.
[18] R. Lang, X. Du, Y. Huang, X. Jiang, Q. Zhang, Y. Guo, K. Liu, B. Qiao, A. Wang, T. Zhang, **n.d.**, DOI 10.1021/acs.chemrev.0c00797.
[19] Y. Tang, C. Asokan, M. Xu, G. W. Graham, X. Pan, P. Christopher, J. Li, P. Sautet, *Nat Commun* **2019**, *10*, 4488.
[20] L. DeRita, J. Resasco, S. Dai, A. Boubnov, H. V. Thang, A. S. Hoffman, I. Ro, G. W. Graham, S. R. Bare, G. Pacchioni, X. Pan, P. Christopher, *Nat Mater* **2019**, *18*, 746–751.
[21] F. Kraushofer, G. S. Parkinson, *Chem Rev* **2022**, *122*, 14911–14939.
[22] Z. Jakub, J. Hulva, M. Meier, R. Bliem, F. Kraushofer, M. Setvin, M. Schmid, U. Diebold, C. Franchini, G. S. Parkinson, *Angewandte Chemie* **2019**, *131*, 14099–14106.

[23] Y. Dai, F. Kong, X. Tai, Y. Zhang, B. Liu, J. Cai, X. Gong, Y. Xia, P. Guo, B. Liu, J. Zhang, L. Li, L. Zhao, X. Sui, Z. Wang, *Electrochemical Energy Reviews* **2022**, *5*, 22.
[24] H.-Y. Zhuo, X. Zhang, J.-X. Liang, Q. Yu, H. Xiao, J. Li, *Chem Rev* **2020**, *120*, 12315–12341.
[25] H. Fei, J. Dong, D. Chen, T. Hu, X. Duan, I. Shakir, Y. Huang, X. Duan, *Chem Soc Rev* **2019**, *48*, 5207–5241.
[26] H. Fei, J. Dong, C. Wan, Z. Zhao, X. Xu, Z. Lin, Y. Wang, H. Liu, K. Zang, J. Luo, S. Zhao, W. Hu, W. Yan, I. Shakir, Y. Huang, X. Duan, *Advanced Materials* **2018**, *30*, 1802146.
[27] L. Zhang, Y. Wang, Z. Niu, J. Chen, *Small Methods* **2019**, *3*, 1800443.
[28] D. Van Dao, L. A. Cipriano, G. Di Liberto, T. T. D. Nguyen, S.-W. Ki, H. Son, G.-C. Kim, K. H. Lee, J.-K. Yang, Y.-T. Yu, G. Pacchioni, I.-H. Lee, *J Mater Chem A Mater* **2021**, *9*, 22810–22819.
[29] M. Zhao, J. Feng, W. Yang, S. Song, H. Zhang, *ChemCatChem* **2021**, *13*, 1250–1270.
[30] S. P, J. John, T. P. D. Rajan, G. M. Anilkumar, T. Yamaguchi, S. C. Pillai, U. S. Hareesh, *J Mater Chem A Mater* **2023**, *11*, 8599–8646.
[31] G. F. S. R. Rocha, M. A. R. da Silva, A. Rogolino, G. A. A. Diab, L. F. G. Noleto, M. Antonietti, I. F. Teixeira, *Chem Soc Rev* **2023**, *52*, 4878–4932.
[32] Y. Wang, X. Wang, M. Antonietti, *Angewandte Chemie International Edition* **2012**, *51*, 68–89.
[33] G. Vilé, D. Albani, M. Nachtegaal, Z. Chen, D. Dontsova, M. Antonietti, N. López, J. Pérez-Ramírez, *Angewandte Chemie International Edition* **2015**, *54*, 11265–11269.
[34] Z. Chen, E. Vorobyeva, S. Mitchell, E. Fako, M. A. Ortuño, N. López, S. M. Collins, P. A. Midgley, S. Richard, G. Vilé, J. Pérez-Ramírez, *Nat Nanotechnol* **2018**, *13*, 702–707.
[35] Y. Wu, C. Li, W. Liu, H. Li, Y. Gong, L. Niu, X. Liu, C. Sun, S. Xu, *Nanoscale* **2019**, *11*, 5064–5071.
[36] H. Li, Y. Wu, L. Li, Y. Gong, L. Niu, X. Liu, T. Wang, C. Sun, C. Li, *Appl Surf Sci* **2018**, *457*, 735–744.
[37] G. Di Liberto, L. A. Cipriano, G. Pacchioni, *ACS Catal* **2022**, 5846–5856.
[38] S. Tosoni, G. Di Liberto, I. Matanovic, G. Pacchioni, *J Power Sources* **2023**, *556*, 232492.
[39] G. Di Liberto, L. A. Cipriano, G. Pacchioni, *ChemCatChem* **2022**, *14*, DOI 10.1002/cctc.202200611.
[40] Y. Huang, J. Xiong, Z. Zou, Z. Chen, *Advanced Materials* **2024**, DOI 10.1002/adma.202312182.
[41] M. Vafaeezadeh, W. R. Thiel, *ChemNanoMat* **2023**, *9*, DOI 10.1002/cnma.202300399.
[42] H. Jiang, W. Yang, M. Xu, E. Wang, Y. Wei, W. Liu, X. Gu, L. Liu, Q. Chen, P. Zhai, X. Zou, P. M. Ajayan, W. Zhou, Y. Gong, *Nature Communications 2022 13:1* **2022**, *13*, 1–9.
[43] W. Zhao, C. Cui, Y. Xu, Q. Liu, Y. Zhang, Z. Zhang, S. Lu, Z. Rong, X. Li, Y. Fang, W. Huang, *Advanced Materials* **2023**, *35*, DOI 10.1002/adma.202301593.
[44] J. Yang, C. Zhu, C.-J. Yang, W.-H. Li, H.-Y. Zhou, S. Tan, X. Liu, D. He, D. Wang, *Nano Lett* **2023**, *23*, 11368–11375.
[45] H. Li, Y. Wu, C. Li, Y. Gong, L. Niu, X. Liu, Q. Jiang, C. Sun, S. Xu, *Appl Catal B* **2019**, *251*, 305–312.
[46] J. Li, Y. Ma, C. Zhang, C. Zhang, H. Ma, Z. Guo, N. Liu, M. Xu, H. Ma, J. Qiu, *Nat Commun* **2023**, *14*, 8146.
[47] A. S. R. Bati, P. Myagmarsereejid, M. Fronzi, K. Fan, P. Liu, Y. L. Zhong, P. L. Burn, I. R. Gentle, P. E. Shaw, M. Batmunkh, *Small Struct* **2024**, *5*, DOI 10.1002/sstr.202300334.
[48] Z. Lian, H. Wu, W. Yang, H. Xiao, L. Ma, J. Zhang, J. Zi, X. Chen, H. Li, *Chem Catalysis* **2023**, *3*, 100824.
[49] H. Li, Q. Li, F. Li, J. Liu, G. Gong, Y. Zhang, Y. Leng, T. Sun, Y. Zhou, S. Han, *Advanced Materials* **2024**, *36*, DOI 10.1002/adma.202308153.
[50] G. Di Liberto, S. Tosoni, G. Pacchioni, *JOURNAL OF PHYSICAL CHEMISTRY LETTERS* **2019**, *10*, 2372–2377.
[51] J. Yu, J. Low, W. Xiao, P. Zhou, M. Jaroniec, *J Am Chem Soc* **2014**, *136*, 8839–8842.
[52] L. Liu, Y. Jiang, H. Zhao, J. Chen, J. Cheng, K. Yang, Y. Li, *ACS Catal* **2016**, *6*, 1097–1108.
[53] S. Sun, P. Gao, Y. Yang, P. Yang, Y. Chen, Y. Wang, *ACS Appl Mater Interfaces* **2016**, *8*, 18126–18131.
[54] J. Zhang, X. Ma, L. Zhang, Z. Lu, E. Zhang, H. Wang, Z. Kong, J. Xi, Z. Ji, *The Journal of Physical Chemistry C* **2017**, *121*, 6133–6140.
[55] J. Low, J. Yu, M. Jaroniec, S. Wageh, A. A. Al-Ghamdi, *Advanced Materials* **2017**, *29*, DOI 10.1002/adma.201601694.
[56] H. Wang, L. Zhang, Z. Chen, J. Hu, S. Li, Z. Wang, J. Liu, X. Wang, *Chem Soc Rev* **2014**, *43*, 5234.
[57] G. Di Liberto, S. Tosoni, G. Pacchioni, *Adv Funct Mater* **2021**, 2009472.
[58] G. Di Liberto, L. A. Cipriano, S. Tosoni, G. Pacchioni, *Chemistry – A European Journal* **2021**, chem.202101764.
[59] I. Grigioni, K. G. Stamplecoskie, E. Selli, P. V. Kamat, *The Journal of Physical Chemistry C* **2015**, *119*, 20792–20800.
[60] Y. Liu, B. R. Wygant, K. Kawashima, O. Mabayoje, T. E. Hong, S. G. Lee, J. Lin, J. H. Kim, K. Yubuta, W. Li, J. Li, C. B. Mullins, *Appl Catal B* **2019**, *245*, 227–239.
[61] P. Li, X. Sui, J. Xu, H. Jing, C. Wu, H. Peng, J. Lu, H. Yin, *Chemical Engineering Journal* **2014**, *247*, 25–32.
[62] S. Zhou, Y. Liu, J. Li, Y. Wang, G. Jiang, Z. Zhao, D. Wang, A. Duan, J. Liu, Y. Wei, *Appl Catal B* **2014**, *158–159*, 20–29.
[63] S. J. A. Moniz, S. A. Shevlin, D. J. Martin, Z. X. Guo, J. Tang, *Energy Environ Sci* **2015**, *8*, 731–759.
[64] I. Grigioni, M. Abdellah, A. Corti, M. V. Dozzi, L. Hammarström, E. Selli, *J Am Chem Soc* **2018**, *140*, 14042–14045.
[65] L. A. Cipriano, G. Di Liberto, S. Tosoni, G. Pacchioni, *The Journal of Physical Chemistry C* **n.d.**, *125*, 11620–11627.
[66] G. Di Liberto, G. Pacchioni, *Journal of Physics: Condensed Matter* **2021**, *33*, 415002.
[67] P. Broqvist, J. F. Binder, A. Pasquarello, *Appl Phys Lett* **2009**, *94*, 141911.
[68] A. Alkauskas, P. Broqvist, F. Devynck, A. Pasquarello, *Phys Rev Lett* **2008**, *101*, 106802.
[69] G. Di Liberto, S. Tosoni, G. Pacchioni, *Adv Funct Mater* **2021**, 2009472.
[70] L. A. Cipriano, G. Di Liberto, S. Tosoni, *Solid State Electron* **2021**, *184*, 108038.
[71] G. Di Liberto, S. Tosoni, *ChemPhysChem* **2023**, *24*, DOI 10.1002/cphc.202200791.
[72] G. Di Liberto, S. Tosoni, G. Pacchioni, *Physical Chemistry Chemical Physics* **2019**, *21*, 21497–21505.
[73] J. Low, J. Yu, M. Jaroniec, S. Wageh, A. A. Al-Ghamdi, *Advanced Materials* **2017**, *29*, 1601694.
[74] G. Di Liberto, S. Tosoni, G. Pacchioni, *Catal Sci Technol* **2021**, *11*, 3589–3598.
[75] Z. Chen, J. Zhao, C. R. Cabrera, Z. Chen, *Small Methods* **2019**, *3*, DOI 10.1002/smtd.201800368.
[76] Z. Chen, S. Mitchell, E. Vorobyeva, R. K. Leary, R. Hauert, T. Furnival, Q. M. Ramasse, J. M. Thomas, P. A. Midgley, D. Dontsova, M. Antonietti, S. Pogodin, N. López, J. Pérez-Ramírez, *Adv Funct Mater* **2017**, *27*, DOI 10.1002/adfm.201605785.
[77] J. Haruyama, T. Ikeshoji, M. Otani, *Phys Rev Mater* **2018**, *2*, 095801.
[78] K. Rigby, J.-H. Kim, *Curr Opin Chem Eng* **2023**, *40*, 100921.
[79] M. C. O. Monteiro, F. Dattila, N. López, M. T. M. Koper, *J Am Chem Soc* **2022**, *144*, 1589–1602.
[80] M. C. O. Monteiro, F. Dattila, B. Hagedoorn, R. García-Muelas, N. López, M. T. M. Koper, *Nat Catal* **2021**, *4*, 654–662.
[81] N. Daelman, M. Capdevila-Cortada, N. López, *Nat Mater* **2019**, *18*, 1215–1221.
[82] G. Di Liberto, G. Pacchioni, Y. Shao-Horn, L. Giordano, *The Journal of Physical Chemistry C* **2023**, *127*, 10127–10133.
[83] G. Kresse, J. Hafner, *Phys Rev B* **1993**, *47*, 558–561.
[84] G. Kresse, J. Furthmüller, *Phys Rev B* **1996**, *54*, 11169–11186.
[85] G. Kresse, J. Furthmüller, *Phys Rev B* **1996**, *54*, 11169–11186.
[86] P. E. Blöchl, *Phys Rev B* **1994**, *50*, 17953–17979.
[87] G. Kresse, D. Joubert, *Phys Rev B* **1999**, *59*, 1758–1775.
[88] J. Heyd, G. E. Scuseria, M. Ernzerhof, *J Chem Phys* **2006**, *124*, DOI 10.1063/1.2204597.
[89] S. Grimme, J. Antony, S. Ehrlich, H. Krieg, *Journal of Chemical Physics* **2010**, *132*, DOI 10.1063/1.3382344.
[90] S. Grimme, S. Ehrlich, L. Goerigk, *J Comput Chem* **2011**, *32*, 1456–1465.
[91] J. P. Perdew, K. Burke, M. Ernzerhof, *Phys Rev Lett* **1996**, *77*, 3865–3868.
[92] S. Nosé, *J Chem Phys* **1984**, *81*, 511–519.
[93] W. G. Hoover, *Phys Rev A (Coll Park)* **1985**, *31*, 1695–1697.
[94] D. Bardelang, F. Camerel, R. Ziessel, M. Schmutz, M. J. Hannon, *J. Mater. Chem.* **2008**, *18*, 489–494.
[95] Y. Wang, X. Wang, M. Antonietti, *Angewandte Chemie International Edition* **2012**, *51*, 68–89.
[96] H. Li, L. Zhou, L. Wang, Y. Liu, J. Lei, J. Zhang, *Physical Chemistry Chemical Physics* **2015**, *17*, 17406–17412.

Entry for the Table of Contents

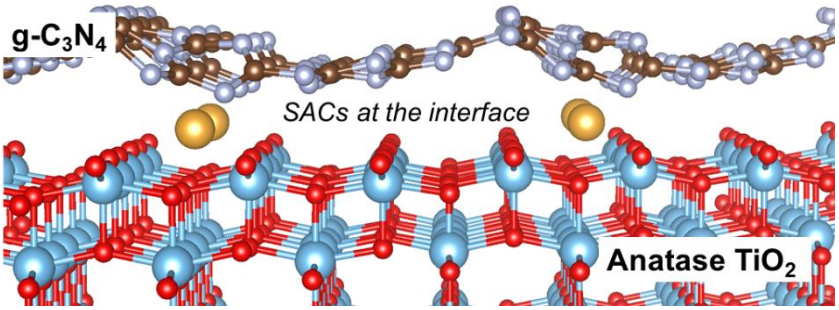

The stabilization of Cu, Ag, and Au single adatoms at the interface between anatase TiO_2 and graphitic carbon nitride is studied with hybrid DFT calculations. On C_3N4/TiO_2, the single metal atoms are ionized and strongly stabilized. The presence of single transition metal atoms is beneficial for the photocatalytic properties of the C_3N4/TiO_2 heterojunction.

Institute and/or researcher Twitter usernames:

Sergio Tosoni: @SergioTosoni3

Università degli Studi di Milano-Bicocca: @unimib